Alternating Hexagonal and Striped Patterns in Faraday Surface Waves

Nicolas Périnet
Faculty of Science, University of Ontario Institute of Technology (UOIT), Oshawa, Ontario, Canada L1H 7K4

Damir Juric
LIMSI-CNRS (UPR 3251), B.P. 133, 91403 Orsay, France

Laurette S. Tuckerman*
*PMMH (UMR 7636 CNRS-ESPCI-UPMC Paris 6-UPD Paris 07), 10 rue Vauquelin, 75005 Paris, France**
(Received 2 May 2012; published 19 October 2012)

A direct numerical simulation of Faraday waves is carried out in a minimal hexagonal domain. Over long times, we observe the alternation of patterns we call quasihexagons and beaded stripes. The symmetries and spatial Fourier spectra of these patterns are analyzed.

DOI: 10.1103/PhysRevLett.109.164501 PACS numbers: 47.20.Ky, 47.20.Ma, 47.54.−r

The Faraday instability [1] describes the generation of surface waves between two superposed fluid layers subjected to periodic vertical vibration. Although these waves usually form crystalline patterns, i.e., stripes, squares, or hexagons, they can form more complicated structures such as quasicrystals or superlattices [2–5]. We have recently carried out the first three-dimensional nonlinear simulations of the Faraday instability [6] and have reproduced the square and hexagonal patterns seen in Ref. [7] with the same physical parameters; see Fig. 1. However, the hexagonal pattern is not sustained indefinitely, but is succeeded by recurrent alternation between quasihexagonal and beaded striped patterns. This long-time behavior is the subject of the present study.

The first detailed spatiotemporal experimental measurements of the interface height $z = \zeta(x, y, t)$ were undertaken by Kityk *et al.* [7]. Their optical technique required the two fluid layers to have the same refractive index, which led them to use fluids of similar viscosities and densities: $\rho_1 = 1346\ \mathrm{kg\,m^{-3}}$, $\nu_1 = 5.35 \times 10^{-6}\ \mathrm{m^2\,s^{-1}}$, $\rho_2 = 949\ \mathrm{kg\,m^{-3}}$, $\nu_2 = 2.11 \times 10^{-5}\ \mathrm{m^2\,s^{-1}}$, and surface tension $\sigma = 35\ \mathrm{mN\,m^{-1}}$. These parameters, especially the density ratio $\rho_2/\rho_1 = 0.7$, differ markedly from most studies of Faraday waves, which use air above either water or silicone oil and so have $\rho_2/\rho_1 \approx 0.001$. At rest, the heavy and light fluids occupy heights of $h_1 = 1.6$ mm and $h_2 = 8.4$ mm, respectively. The imposed vibration has frequency $f = 12$ Hz and the Faraday instability leads to subharmonic standing waves, so that $\zeta(x, y, t)$ oscillates with period $T = 2/f = 0.1666$ s. Floquet analysis [8] for these parameters yields a critical wavelength of $\lambda_c = 2\pi/k_c = 13.2$ mm, with which the experiments show close agreement [7]. Thus, another atypical feature of this parameter regime is that $h_1 \ll \lambda_c$; see Fig. 1. Floquet analysis also yields a critical acceleration of $a_c = 25.8\ \mathrm{m\,s^{-2}} = 2.63g$. Our simulations are carried out at $a = 38.0\ \mathrm{m\,s^{-2}} = 3.875g = 1.473a_c$, for which hexagons were observed experimentally [7].

We summarize our formulation and the numerical methods used to compute the fluid motion; see Ref. [6] for a more detailed description. Our computations use a single-fluid model, representing the velocity $\mathbf{u}$ and pressure p over the whole domain on a staggered Marker and Cell mesh [9] which is fixed and uniform. The viscosity and density are variable, taking the values ν_1, ρ_1 for the denser lower fluid and ν_2, ρ_2 for the lighter upper fluid, and varying over a few gridpoints at the interface. The moving

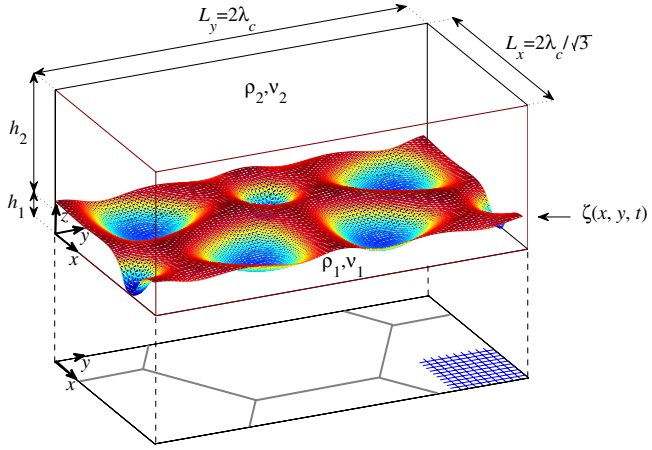

FIG. 1 (color online). Above: instantaneous realization of hexagaonal Faraday waves in a domain of size $L_x \times L_y \times (h_1 + h_2)$. The density and viscosity are ρ_2, ν_2 above the free surface at $z = \zeta(x, y, t)$; below, they are ρ_1, ν_1. The displacement amplitude of ζ is comparable to h_1; at its lowest points, ζ almost touches the lower boundary. Below: projection of the horizontal doubly periodic rectangular domain of dimensions $L_x \times L_y = 2\lambda_c/\sqrt{3} \times 2\lambda_c$ shows that it is compatible with a hexagonal lattice. The minima of ζ (above) are located at the vertices and centers of the hexagons (below). The right corner represents a portion of the rectangular computational grid; the actual grid is twice as fine in each direction.

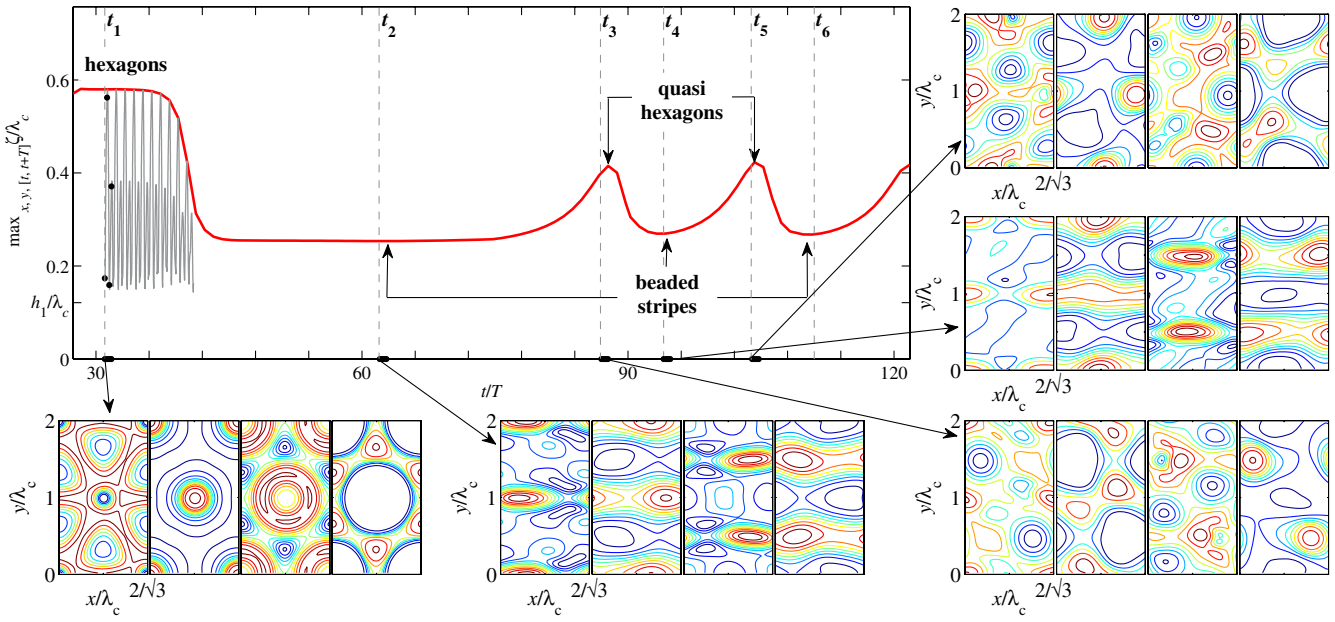

FIG. 2 (color online). Maximum interface heights $\max_{x,y}\zeta(x, y, t)$ (rapidly oscillating curve) and $\max_{x,y,[t,t+T]}\zeta(x, y, t)$ (smooth envelope). Surrounding visualizations show instantaneous contour plots of $\zeta(x, y, t)$ at times indicated by black dots on rapidly oscillating curve and along abscissa. The range of contour levels is scaled independently for each plot. Over the large white areas, the interface is very close to the bottom and almost flat. Visualizations shown at $t_i + jT/4$ for $j = 0, 1, 2, 3$ (i.e., over one subharmonic period) for hexagons at t_1, symmetric and nonsymmetric beaded stripes at t_2 and t_4, and quasihexagons at t_3 and t_5.

interface, defined by $z = \zeta(x, y, t)$, is computed by a front-tracking [10] or immersed boundary [11] method on a semi-Lagrangian triangular mesh which is fixed in the horizontal x and y directions and moves along the vertical direction z. The interface is advected and the density and viscosity fields updated. The capillary force is computed locally on the Lagrangian mesh and included in the Navier-Stokes equations, which are solved by a projection method. The computations are carried out in the oscillating reference frame of the container by adding a time-periodic vertical acceleration $a\sin(2\pi ft)\mathbf{e}_z$ to the equations of motion. No-slip boundary conditions are imposed at the top and bottom boundaries, while periodic boundary conditions are used at the vertical boundaries.

The horizontal dimensions of the domain are chosen to accommodate a hexagonal pattern. We take $L_x = 2\lambda_c/\sqrt{3}$ and $L_y = 2\lambda_c$, as shown in Fig. 1, so that large-scale spatial variations are inaccessible. This domain is also compatible with striped or rectangular patterns, as will be discussed below. The simulations were run with a spatial resolution of $N_x \times N_y \times N_z = 58 \times 100 \times 180$. Each horizontal rectangle is subdivided into 64 triangles to represent the interface. To validate the spatial discretization, we repeated the simulations with a finer resolution of $N_x \times N_y \times N_z = 75 \times 125 \times 225$. Although small quantitative changes were seen, the dynamics remained qualitatively unchanged. The time step is limited by the advective step, taking values varying between $T/24\,000$ for a hexagonal pattern and $T/4000$ for a beaded striped pattern. This makes the simulation of behavior over many subharmonic periods extremely time consuming.

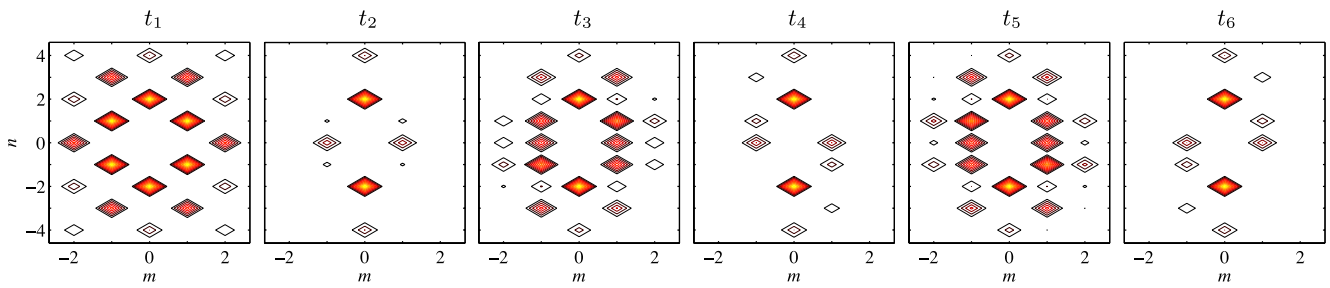

FIG. 3 (color online). Time-filtered spatial Fourier spectra $\zeta_{mn}(t_i)$: hexagons at t_1, beaded stripes at t_2, quasihexagons at t_3 and t_5, nonsymmetric beaded stripes at t_4 and t_6.

Starting from zero velocity and an initial random perturbation of the flat interface, our simulations produced a hexagonal pattern which oscillates subharmonically with the same spatiotemporal spectrum as Ref. [7], as detailed in Ref. [6]. In the experiments, hexagons are transient and difficult to stabilize [12], competing with squares and disordered states [7,13]. In our simulations, after about ten subharmonic periods, we observed a drastic departure from hexagonal symmetry. Figure 2 shows the instantaneous maximum height $\max_{x,y}\zeta(x, y, t)$ and its envelope $\max_{x,y,[t,t+T]}\zeta(x, y, t)$. Surrounding the time-evolution plot are contours of the interface height at representative times over one subharmonic cycle.

At times $t_1 + jT/4$, the patterns are hexagonal. Each is invariant under rotations by $\pi/3$ and under reflection, for example, about $y = n\lambda_c$; these operations generate their isotropy subgroup (group of symmetries), which is isomorphic to D_6. We call the patterns at $t_2 + jT/4$ beaded stripes. They satisfy the two symmetry relations

$$\zeta(x, n\lambda_c - y) = \zeta(x, y) = \zeta(m\lambda_c/\sqrt{3} + \tilde{x}_0 - x, y + n\lambda_c), \tag{1}$$

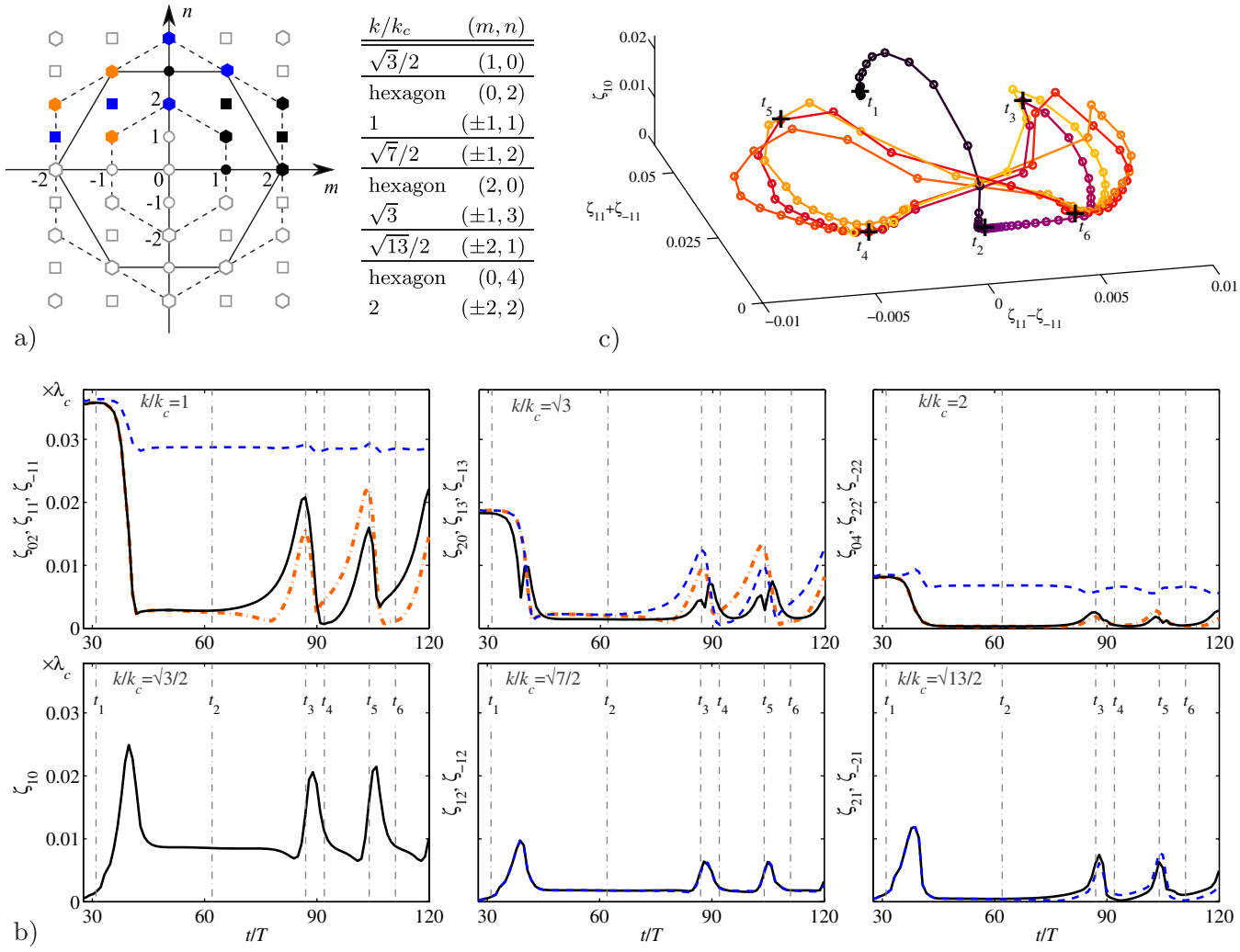

FIG. 4 (color online). (a) Spatial Fourier grid of the domain. Hexagonal symbols: sets of six $\mathbf{k}_{mn}$ which share the same length k. This portion of the grid contains three hexagons, with $k/k_c = 1$, $\sqrt{3}$, and 2. The hexagonal modes are located at the vertices (and not the sides) of the large hexagons indicated by solid and dashed lines. Square symbols: sets of four $\mathbf{k}_{mn}$ which share the same k. Circles: other modes. Colors differentiate between $\mathbf{k}_{mn}$ and its images under rotations of $l\pi/3$ for hexagonal modes or under reflections across the n axis for the others. (b) Temporal evolution of $\zeta_{mn}(t)$, grouped by length k. The color code is that used in the spatial Fourier grid. Dashed blue curves: hexagonal modes (0, 2), (1, 3), (0, 4) and nonhexagonal modes (−1, 2), (−2, 1). Solid black curves: hexagonal modes (1, 1), (2, 0), (2, 2) and nonhexagonal modes (1, 0), (1, 2), (2, 1). Dash-dotted orange curves: hexagonal modes (−1, 1), (−1, 3), (−2, 2). (c) Three-dimensional phase portrait of temporal evolution of modes for an extended simulation. Points are equally spaced in time; their color evolves in time from dark to light. Times $t_1, \ldots, t_6$ marked by crosses and by vertical lines in (b).

where $\tilde{x}_0 \approx \lambda_c/(2\sqrt{3})$ is a spatial phase. The second equality in Eq. (1) is variously called shift-and-reflect or glide-reflection symmetry. These invariances describe the crystallographic group called *pmg* and *p2mg* [13,14], which is isomorphic to $Z_2 \times Z_2$. At later times, the patterns have no exact symmetries. Nevertheless, the patterns at times $t_3 + T/4$ and $t_5 + 3T/4$ contain large flat cells surrounded by six small peaks like those at $t_1 + 3T/4$ which lead us to call them quasihexagons. Quasihexagons at t_3 and t_5 appear in two distinct forms, which are related by the spatiotemporal symmetry

$$\zeta(m\lambda_c/\sqrt{3} + x_0 - x, y + y_0, t_3 + T/2) = \zeta(x, y, t_5) \qquad (2)$$

with phases $x_0 \approx 0.7\lambda_c/\sqrt{3}$ and $y_0 \approx \lambda_c/2$. The patterns at t_4 and t_6 resemble those at t_2 but do not satisfy Eq. (1); we call these nonsymmetric beaded stripes. These are also related by the spatiotemporal symmetry [Eq. (2)].

To quantify the behavior in Fig. 2, we have studied the spatial Fourier spectrum. The rectangular box of Fig. 1 constrains the wave vectors to lie on the grid $\mathbf{k}_{mn} \equiv (\sqrt{3}m\mathbf{e}_x + n\mathbf{e}_y)k_c/2$, where $m, n \in \mathbb{Z}$, as shown in Figs. 3 and 4(a). We define the time-filtered spatial Fourier transform

$$\frac{\zeta(\mathbf{x}, t)}{\lambda_c} = \sum_{m,n} e^{i\mathbf{k}_{mn}\cdot\mathbf{x}}\hat{\zeta}_{mn}(t), \qquad \zeta_{mn}(t) \equiv \max_{[t,t+T]}|\hat{\zeta}_{mn}(t)|.$$

In Fig. 3, we plot $\zeta_{mn}(t_i)$ for $t_1, \ldots, t_6$. For the hexagonal pattern at time t_1 the modes with non-negligible amplitude are those belonging to hexagons, primarily $(m, n) = (\pm 1, \pm 1)$ and $(0, \pm 2)$, with $k/k_c = 1$, but also $(\pm 2, 0)$ and $(\pm 1, \pm 3)$, with $k/k_c = \sqrt{3}$, and $(0, \pm 4)$ and $(\pm 2, \pm 2)$, with $k/k_c = 2$. The spectrum at t_2 is dominated by modes $(0, \pm 2)$ and $(\pm 1, 0)$, which combine to form the beaded striped patterns—with one bead over L_x and two stripes over L_y—seen in Fig. 2 at t_2. The spectra at t_3 and t_5 combine wave numbers seen at t_1 and t_2, while those at t_4 and t_6 are asymmetric versions of that at t_2. The spatiotemporal symmetry [Eq. (2)] is manifested by $\zeta_{-m,n}(t_{3,4}) = \zeta_{mn}(t_{5,6})$.

Figure 4(b) shows the time evolution of $\zeta_{mn}(t)$ for the dominant wave vectors, grouping those with the same k value into a single graph. Because $\zeta_{m,-n} = \zeta_{-m,n}$ (resulting from the reality condition $\hat{\zeta}_{m,-n} = \hat{\zeta}^*_{-m,n}$), we plot only positive n. We first describe the evolution of the four most dominant modes in the leftmost column. During the hexagonal phase at t_1, the only modes with non-negligible amplitude are those belonging to hexagons. At $t/T \approx 40$, these drop abruptly, with the exception of ζ_{02}. This is accompanied by a burst in amplitude of some of the nonhexagonal modes, notably ζ_{10}, followed by its saturation. Shortly after t_2, $\zeta_{1,1}$ begins to rise, followed by $\zeta_{-1,1}$. Eventually ζ_{10} rises as well; we conjecture that its growth is fueled by mode interactions arising from $\mathbf{k}_{11} + \mathbf{k}_{-1,-1} + \mathbf{k}_{1,0} = \mathbf{k}_{10}$. By t_3, these have attained values which approach ζ_{02}, leading to the quasihexagonal patterns at t_3. Mode amplitudes $\zeta_{\pm 1,1}$ then fall quickly, followed by $\zeta_{1,0}$, leading again to a short-lived beaded striped pattern at time t_4. The cycle then repeats, but this time $\zeta_{-1,1}$ rises before $\zeta_{1,1}$ and attains a higher peak at time t_5, leading to the difference between the quasihexagonal patterns at t_5 and t_3. The next cycle shows ζ_{11} leading again at t_6. Most of the higher k modes behave like their lower k analogs.

Figure 4(c) shows a phase portrait, projecting the dynamics onto coordinates $\zeta_{11} + \zeta_{-1,1}$, $\zeta_{11} - \zeta_{-1,1}$, and ζ_{10} to represent the dynamics. Here, the simulation has been extended and shows several additional repetitions. The concentration of points indicates that the hexagonal pattern at time t_1 and the beaded striped pattern at t_2 are saddles. Afterwards, the trajectory consists of two crossed loops connecting t_3, t_4, t_5, and t_6. Several dynamical-systems scenarios lead to limit cycles which visit symmetrically related sets, e.g., Hopf bifurcations [15] or heteroclinic cycles [16]. Since the saddles at t_1 and t_2 are not part of the periodic cycle, nor its center, our planned investigation of its origin will be challenging.

A complete analysis of the general bifurcation problem on a hexagonal lattice [17,18] shows that the patterns at onset are hexagons and stripes. This analysis of steady states on a hexagonal grid does not apply directly to our study of subharmonic standing waves on the rectangular lattice of Fig. 1. At the other extreme, in large-domain experiments, hexagonal patterns are often observed to undergo other spatiotemporal dynamics, such as competition with squares [7,13,19], which are inaccessible to current mathematical analysis and to our simulation.

We have observed complex long-time temporal behavior in a fully resolved three-dimensional simulation of Faraday waves in the minimal domain which can accommodate a hexagonal pattern. Although this scenario may prove to be replaced by other dynamics in large domains, we believe that it is of interest in its own right and that it may well be applicable to other pattern-forming systems.

We thank P.-L. Buono and M. Golubitsky for sharing their knowledge of symmetry and C. Wagner for in-depth remarks on experiments. N. P. was partly supported by the Natural Sciences and Engineering Research Council of Canada.

*laurette@pmmh.espci.fr

[1] M. Faraday, Phil. Trans. R. Soc. London **121**, 299 (1831).
[2] B. Christiansen, P. Alstrøm, and M. T. Levinsen, Phys. Rev. Lett. **68**, 2157 (1992).
[3] W. S. Edwards and S. Fauve, Phys. Rev. E **47**, R788 (1993).
[4] A. Kudrolli, B. Pier, and J. P. Gollub, Physica (Amsterdam) **123D**, 99 (1998).

[5] A. M. Rucklidge, M. Silber, and A. C. Skeldon, Phys. Rev. Lett. **108**, 074 504 (2012).
[6] N. Périnet, D. Juric, and L. S. Tuckerman, J. Fluid Mech. **635**, 1 (2009).
[7] A. V. Kityk, J. Embs, V. V. Mekhonoshin, and C. Wagner, Phys. Rev. E **72**, 036 209 (2005); **79**, 029 902(E) (2009).
[8] K. Kumar and L. S. Tuckerman, J. Fluid Mech. **279**, 49 (1994).
[9] F. H. Harlow and J. E. Welch, Phys. Fluids **8**, 2182 (1965).
[10] G. Tryggvason, B. Bunner, A. Esmaeeli, D. Juric, N. Al-Rawahi, W. Tauber, J. Han, and Y.-J. Jan, J. Comput. Phys. **169**, 708 (2001).
[11] C. S. Peskin, J. Comput. Phys. **25**, 220 (1977).
[12] C. Wagner (private communication).
[13] C. Wagner, H. W. Müller, and K. Knorr, Phys. Rev. E **62**, R33 (2000); **68**, 066 204 (2003).
[14] http://en.wikipedia.org/wiki/Wallpaper_group.
[15] T. Clune and E. Knobloch, Physica (Amsterdam) **74D**, 151 (1994).
[16] P.-L. Buono, M. Golubitsky, and A. Palacios, Physica (Amsterdam) **143D**, 74 (2000).
[17] E. Buzano and M. Golubitsky, Phil. Trans. R. Soc. A **308**, 617 (1983).
[18] M. Golubitsky, J. Swift, and E. Knobloch, Physica (Amsterdam) **10D**, 249 (1984).
[19] B. Abou, J.-E. Wesfreid, and S. Roux, J. Fluid Mech. **416**, 217 (2000).